*Progress In Electromagnetics Research C, Vol. 60, 83–93, 2015*

# Phase Enhancement for Multi-Resonance Compact Metamaterial Antennas

**Mahmoud A. Abdalla[1, *], Ahmed A. Ibrahim[2], and Mohammed H. Abd El-Azeem[3]**

**Abstract**—In this paper, a nonlinear phase enhancement of multi-resonance composite right/left-handed unit cell for multi-band antennas is presented. Different antennas with nonlinear enhanced phase which can operate up to five different frequency bands are introduced. Meanwhile, the proposed antennas have compact size so that they can demonstrate size reduction up to 60% compared to conventional patch antennas operating at the same frequencies. The achieved phase enhancement has been validated by comparing two different configurations of composite right/left-handed cells. The analysis, electromagnetic full wave simulations and experimental results are discussed. A reasonable agreement is achieved between the measured and simulated results.

## 1. INTRODUCTION

The rapid growth of the wireless communication systems leads to integration of different wireless services in one terminal. These applications demand antennas with special characteristics such as small size, multi-band and high performance [1]. Multi-band antennas have drawn great attention in recent years because one antenna can cover several frequency bands. Several researches have contributed to designing multi-band antennas. Different techniques for designing multi-band antennas such as adopting multi-branched strips [2, 3] and adding parasitic elements to resonate at different frequencies in a single radiating device [4, 5]. However, these solutions generally suffer from certain drawbacks including a large volume and large ground plane.

Since the introduction of the artificial composite right/left-handed (CRLH) metamaterial (MTM) transmission line (TL), it has gained great interest from electromagnetic community.

Basically, CRLH TL is characterized by anti-parallel phase and group velocities, non-linear progressive phase properties and many other wave propagation properties [6–8]. This has helped the electromagnetic researchers with more design capabilities than conventional (right handed) transmission line. Accordingly, CRLH TL has been used in introducing many compact and multi-band microwave components [9–12], to name some examples such as impedance transformers [13], power divider [14], resonators [15], filters [16], couplers [17], radar absorber [18].

On the other hand, many CRLH TL based antennas including resonant, zeroth order antenna and leaky wave antennas have been suggested [19–22]. Making use of these approaches, many attempts for multi-band antennas have been presented [23–28].

In this paper, different CRLH TL metamaterial multi-resonance antennas are introduced. The proposed antennas are compact and can serve dual, triple, quad and five bands. The compactness of the proposed antennas is achieved by making use of the nonlinear behavior of the CRLH TL. The theoretical concepts of the designed antenna are discussed. The performance of the designed antennas has been validated using commercial software CST microwave studio. Finally, the simulated results are confirmed by experimental measurements.

*Received 22 August 2015, Accepted 9 November 2015, Scheduled 7 December 2015*

* Corresponding author: Mahmoud Abdelrahman Abdalla (maaabdalla@ieee.org).

[1] Electronic Engineering Department, MTC College, Cairo, Egypt. [2] Communications and Electronic Department, Faculty of Engineering, Minia University, El-Minia, Egypt. [3] Electronics and Communication Engineering Department, Arab Academy for Science, Technology and Maritime Transport, Cairo, Egypt.

## 2. MULTI-BAND CRLH ANTENNA THEORY

The equivalent circuit of one unit cell of CRLH TL is shown in Fig. 1 where $L_R$ and $C_R$ represent the hosting TL parasitic elements whereas $L_L$ and $C_L$ are the loading elements. The overall per unit length transmission line impedance ($Z$) and admittance ($Y$) are expressed as

$$Z = j\omega L'_R + 1/\left(j\omega C'_L\right) \tag{1}$$

$$Y = j\omega C'_R + 1/\left(j\omega L'_L\right) \tag{2}$$

where $L'_L$ and $C'_L$ are the times length elements, and $L'_R$ and $C'_R$ are the per unit length elements. In the case that the resonances of the series of branch and shunt branch are equal, this used to be called a balanced CRLH TL; otherwise it is unbalanced CRLH TL.

The dispersion equation of the CRLH TL can be extracted by applying the periodic analysis of infinite number of cells of length ($d$) [29]. This can be derived as

$$\cos(\beta d) = \cos(\theta) + \frac{1}{2}ZY\cos^2\left(\frac{\theta}{2}\right) + i\frac{1}{2}\left(Z_oZ + Y_oY\right)\sin\left(\frac{\theta}{2}\right) \tag{3}$$

where $Z_0$ and $Y_0$ are the right-handed characteristic impedances and admittances, respectively. Also, $Z$ is the series added capacitive load, $Y$ the shunt inductive load, and $\theta$ the hosting transmission line electrical length. It is worth to comment that assuming that the periodic length of the unit cells is much smaller than the hosting TL wavelength ($d \ll \lambda \to 0$), the progressive phase shift can be extracted as

$$\cos(\beta d) = 1 - \frac{\omega^2 d^2}{2}\left[\left(L'_R - \frac{1}{\omega^2 C'_L}\right)\left(C'_R - \frac{1}{\omega^2 L'_L}\right)\right] \tag{4}$$

The dispersion diagram for the CRLH TL is illustrated in Fig. 2(a) for unbalanced CRLH TL and in Fig. 2(b) for balanced CRLH TL.

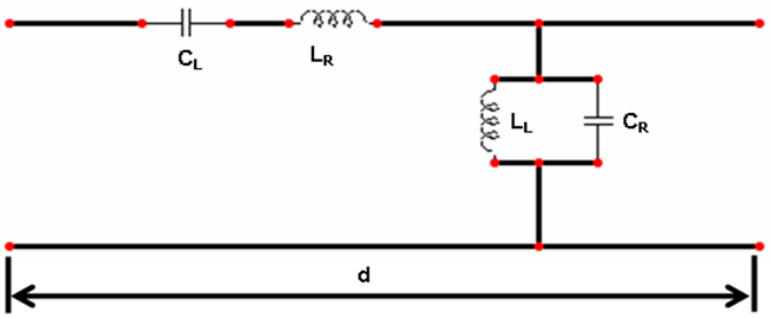


**Figure 1.** The equivalent circuit model of CRLH transmission line.

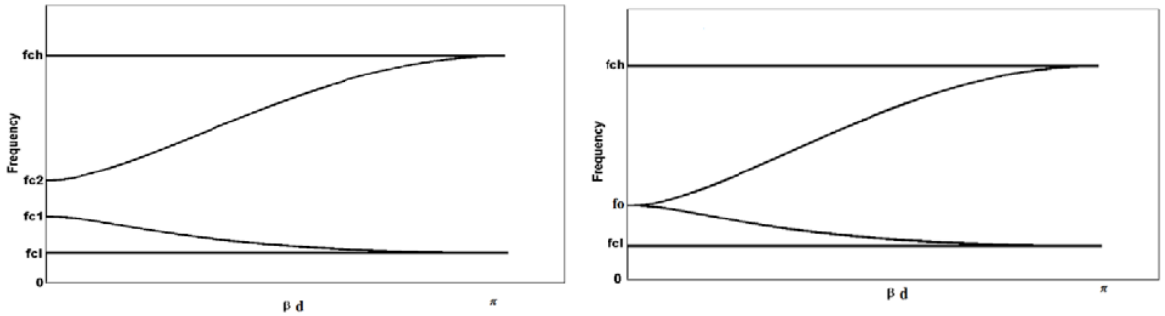


(a) (b)

**Figure 2.** The dispersion diagram of a (a) unbalanced CRLH transmission line, (b) balanced CRLH transmission line.

As shown in the figures, the CRLH TL has a left-handed (LH) passband at low frequencies and a right-handed (RH) passband at higher frequencies. The condition, $\beta d = \pi$, yields the cutoff frequency for the onset of the left-handed propagation ($f_{cl}$), at lower frequencies, and also for the end of the right-handed propagation ($f_{ch}$), at higher frequencies as follow

$$4 = \omega^2 d^2 \left(L'_R - \frac{1}{\omega^2 C'_L}\right)\left(C'_R - \frac{1}{\omega^2 L'_L}\right) \tag{5}$$

$$f_{cl} \approx \frac{1}{4\pi}\frac{1}{\sqrt{L_L C_L}}, \quad f_{ch} \approx \frac{1}{\pi}\frac{1}{\sqrt{L_R C_R}} \tag{6}$$

The condition, $\beta d = 0$, yields the cutoff frequency for the end of the LH propagation ($f_{c1}$) and also for the onset of the RH propagation ($f_{c2}$) as follow

$$\left(L'_R - \frac{1}{\omega^2 C'_L}\right)\left(C'_R - \frac{1}{\omega^2 L'_L}\right) = 0 \tag{7}$$

$$f_{c1} = \min\left(\frac{1}{2\pi}\frac{1}{\sqrt{L'_L C'_R}}, \frac{1}{2\pi}\frac{1}{\sqrt{L'_R C'_L}}\right), \quad f_{c2} = \max\left(\frac{1}{2\pi}\frac{1}{\sqrt{L'_L C'_R}}, \frac{1}{2\pi}\frac{1}{\sqrt{L'_R C'_L}}\right) \tag{8}$$

The characteristic impedance of the CRLH TL can be extracted using the line series impedance ($Z$) and shunt admittance ($Y$) in Eqs. (1) and (2) as

$$Z_{CRLH} = \sqrt{\frac{Z}{Y}} = \sqrt{\frac{j\omega L'_R + 1/j\omega C'_L}{j\omega C'_R + 1/j\omega L'_L}} \tag{9}$$

Balanced CRLH TL can be considered as a cascade of two matched LH TL, with $Z_L$, and RH TL, with $Z_{R,}$ i.e., ($Z_{CRLH} = Z_R = Z_L$) as

$$Z_{CRLH} = Z_{LH} = \sqrt{\frac{L'_L}{C'_L}} = Z_{RH} = \sqrt{\frac{L'_R}{C'_R}} \tag{10}$$

Also, the progressive phase shift along a balanced CRLH TL has a simplified formula that can be represented as the superposition of LH and RH phase sections as

$$\phi_{CLRH} = -\beta d = \left(\frac{1}{\omega\sqrt{C'_L L'_L}} - \omega\sqrt{C'_R L'_R}\right) d \tag{11}$$

Based on above mathematical explanation, a balanced CRLH TL can have a wide passband with nonlinear phase shift within it. Also, it is clear that the cutoff frequencies of all these bands are controlled by the values of LH elements and RH transmission line elements. In consequence, these values can control the phase shift. Based on these properties, CRLH TLs can be utilized to introduce multiband antennas.

Conventional microstrip patch antenna can introduce a resonance at frequency corresponding to half wavelength. Therefore, multi-bands are possible only at integer multiple harmonic frequencies due to the linear phase dependence in RH TLs. On the other hand, by employing the nonlinear properties of CRLH TL, arbitrary multi-band functionality can be obtained. This can be adjusted by using $N$ cells CRLH TL as follow

$$Phase = \phi_l + \phi_R = -\beta_L d_L - \beta_R d_R = \left(\frac{N}{\omega\sqrt{C_L L_L}}\right) - \left(N\omega\sqrt{C_R L_R}\right) = n\pi \tag{12}$$

where $n$ is an arbitrary integer and $N$ the number of used cells. In practice, increasing the number of cells increases the progressive phase shift and hence increases the possible number of bands. By investigating (11), it is obvious that the dominant nonlinear term is the first term ($N/\omega\sqrt{C_L L_L}$) which can be designed to be more dominant by either increasing $N$, decreasing the loading elements ($C_L$ or $L_L$). However, increasing $N$ will increase the antenna size. Decreasing the loading elements values will increase the lower left-handed frequency ($f_{cl}$), in Eq. (9), which again will increase the antenna operating frequencies, which in turns will increase the antenna electrical size. In fact, a tradeoff has

to been considered to use smaller size of antenna cells with more bands. To do this, we have to select loading element ($C_L$ or $L_L$) that contributes more in the radiation properties. Then the other element will be treated in a tradeoff scenario between its value and number of cells. This will be explained in the following sections.

## 3. DUAL/TRIPLE COMPACT CRLH ANTENNA

In this section, we introduce the phase enhancement by controlling the loading shunt inductor in single cell CRLH antenna to introduce a dual/triple band instead of single band using a non-enhanced phase CRLH cell antenna. Also, our optimized phase work aims to introduce more bands at lower frequencies compared to non-optimized phase. This in turn will enhance and decrease the electrical length of the antenna for the same physical size.

Through our designs presented in this section, the antennas are printed on an FR4 substrate with relative permittivity = 4.4, dielectric loss tangent = 0.025 and thickness ($h$) = 1.6 mm. The two antennas were designed to be matched to a 50 Ω RH feeding TL. The performances of two different antennas were investigated by full wave simulation and measurements for the completeness of work.

### 3.1. Single Cell CRLH Antenna Structure

The 2D layout of single band, non-enhanced phase one-cell CRLH antenna is shown in Fig. 3(a). As shown in the figure, the antenna satisfies the CRLH equivalent circuit in Fig. 1 by using a series interdigital capacitor and grounded shunt stub inductor. On the other hand, Fig. 3(b) illustrates the 2D layout of the enhanced phase one-cell CRLH antenna whose shunt inductor is realized using only grounded shunt vias. Comparing the two configurations, we can claim that the last configuration has smaller shunt inductor ($L_L$) which will increase the contribution of the left-handed phase term in Eq. (11) and increase the lower cutoff frequency of the left-handed passband as in Eq. (5).

The design of antenna in Fig. 3(a) was started by achieving zero order resonance antenna (ZORA) using the stub antenna at 2.4 GHz. Also, the antenna elements were designed to demonstrate 50 Ω as in Eq. (9). Accordingly, the loading elements $C_L$ and $L_L$ have been calculated (using Eq. (11)) for $N = 1$. It is worth to comment that $C_R$ and $L_R$ are calculated as parasitic elements for 20 mm transmission line. Hence the interdigital capacitor and stub inductor dimensions are obtained as [30]

$$C(\text{pF}) = 3.937 \times 10^{-5} l_f \left(\varepsilon_r + 1\right) \left(0.11 \left(n - 3\right) + 0.252\right) \tag{13}$$

where $l_f$ is interdigital capacitor length in micrometer

$$L_L = Z_0 \tan\left(\beta l_s\right) / \omega \tag{14}$$

where $l_s$ is the stub length, and $Z_0$ and $\beta$ are the characteristic impedance and propagation constant, corresponding to the stub width, respectively. For the sake of fabrication limitation, the finger width and separations were kept undersigned = 0.2 mm. Hence, the interdigital finger length is 9 mm.

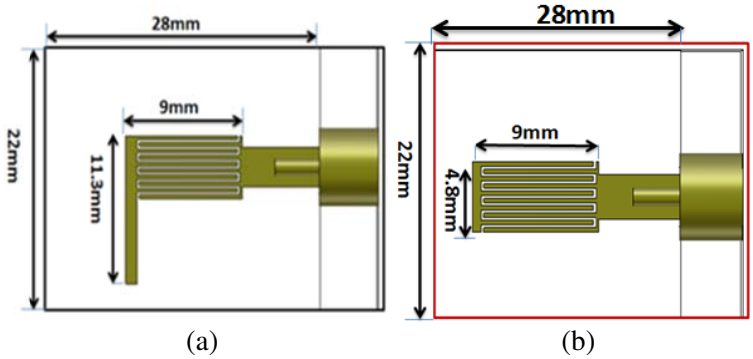


**Figure 3.** The layout of Unit cell CRLH antenna. (a) With stub. (b) With stub-less.

The CRLH parameters of the unit cell transmission line are calculated using Equations (13) and (14). The value for $C_l$ is 1.4 pF, and $L_l$ is 3.4 nH. Also the values of $C_R$ and $L_R$ were calculated based on transmission line theory, and they are found equal to 1.8 nH and 1.8 pF, respectively. For validation of the calculations, a two-port unit cell CRLH transmission line with stub is simulated using CST and compared with the circuit simulation as shown in Fig. 4(a). It is clear that good agreement is achieved between the circuit and full wave simulations. To confirm the balanced and zeroth order mode, the dispersion diagram of the unit cell transmission line is studied and illustrated in Fig. 4(b). It is obvious that this unite cell works as balanced transmission line with zero order at 2.3 GHz. So changing this transmission line to antenna by removing the second port as shown in Fig. 3(a), we expect that the antenna will resonate around 2.3 GHz.

On the other hand, upon using non-stub in Fig. 3(b), the shunt inductor can be expressed as a simple via inductor whose value can be calculated as

$$L_L = \mu h \tag{15}$$

where $\mu$ is the substrate permeability and $h$ the substrate thickness.

For the precalculated $C_L$ and new $L_L$ in Eq. (14), the left-handed phase has been enhanced to demonstrate more than one operating frequency. In other words, from the structure point of view, by removing the stub, we can avoid the phase delay. At the end, this helps the designer for better control of the total left- and right-handed phase delay which adds more possible operating bandwidths.

This can be illustrated in Fig. 5 where the simulated reflection coefficient is shown for the two antenna configurations. As shown in the figure, the stub CRLH cell based antenna can demonstrate only one resonance at 2.4 GHz with reflection coefficient = −14 dB and 10 dB bandwidth = 50 MHz, approximately. On the other hand, the proposed one cell CRLH without using stub can demonstrate triple-band operation at 2.2 GHz, 3 GHz and 3.6 GHz. The reflection coefficient at the first band (2.2 GHz) of the proposed antenna is −6 dB which may be considered an operating band. At the two other frequencies (3 GHz and 3.6 GHz), the reflection coefficient becomes (−15 dB and −20 dB, respectively) with approximate 10 dB bandwidth = 50 MHz and 80 MHz, respectively. Analyzing the two previous results, we can conclude the following: the proposed stub-less antenna with lower shunt inductance compared to the stub has shifted the zeroth order mode from 2.4 GHz to 3 GHz which is illustrated in Fig. 4 by $na = 0$ and $nb = 0$, respectively. A new resonance mode at 2.2 GHz is modeled as the mode $nb = -1$ to refer to mode in the LH passband. Hence, the resonance frequency at 3.6 GHz should demonstrate the right-handed passband with first order ($nb = 1$).

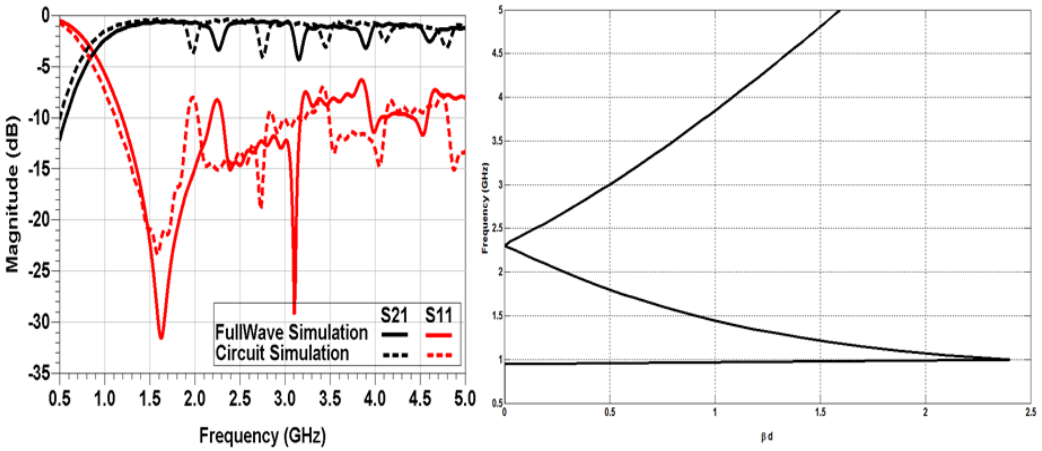


(a) (b)

**Figure 4.** Unit cell CRLH transmission line. (a) $S$-parameters. (b) Dispersion diagram.

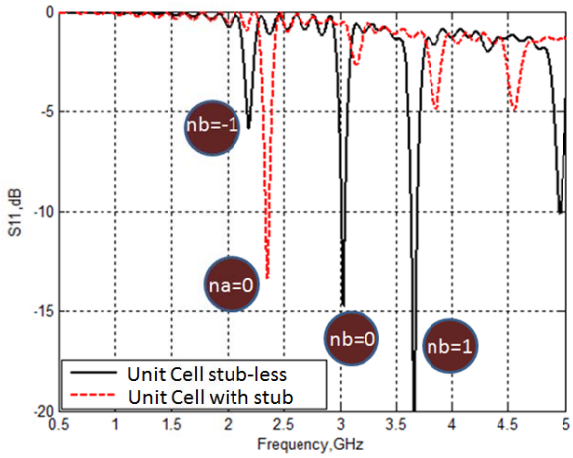


**Figure 5.** The simulated reflection coefficient of the stub CRLH antenna (symbol a) and the stub-less CRLH antenna (symbol (b)).

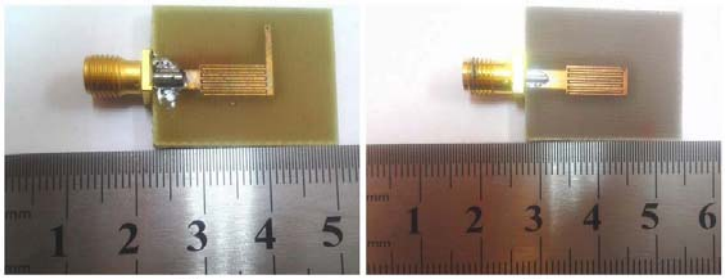

(a) (b)

**Figure 6.** The fabricated 1 cell CRLH antenna. (a) With stub. (b) With stub-less.

### 3.2. Single Cell CRLH Antenna — Measurements

Photographs of the fabricated two antennas are shown in Fig. 6. The simulated and measured return losses of the antenna with stub are shown in Fig. 7(a). From the measured result, it is obvious that the antenna can achieve better than −14 dB reflection coefficient at 2.4 GHz with 50 MHz bandwidth. Also good agreement between measured and simulated results is achieved. On the other hand, the results of the stub-less antenna are demonstrated in Fig. 7(b). It is clear from the measured results that the antenna can resonate at three bands at 2.2 GHz, 3 GHz and 3.7 GHz with reflection coefficient equal to −6 dB, −12 dB and −18 dB, respectively. Similarly, good agreement between simulated and measured results is obvious. There is a small frequency shift at the third band which can be claimed due to fabrication process.

To confirm this claim about the phase enhancement in the stub-less antenna, the two antennas with two ports have been simulated, and the transmission coefficient ($S_{21}$) phase is plotted in Fig. 8. As shown in the figure, the stub-less CRLH cell phase is larger than the stub configuration. Also, it can cross the zero three times compared to only one for stub CRLH cell. That can support the possibility of the proposed stub-less configuration to demonstrate more than one operating frequency introduced before in Fig. 5. Although the three operating frequencies are shifted from those in designing the antenna, they still confirm the number of antenna operating frequencies.

Finally, in the case of restricting the band definition to introduce −10 dB, we can claim that the optimized phase antenna becomes dual band compared to original one; otherwise, the proposed antenna is triple-band. This conclusion can be interpreted as that both antenna designs can achieve the resonance at different orders. Moreover, based on the same physical antenna dimension, we can confirm the antenna electrical length reduction thanks to the first band.

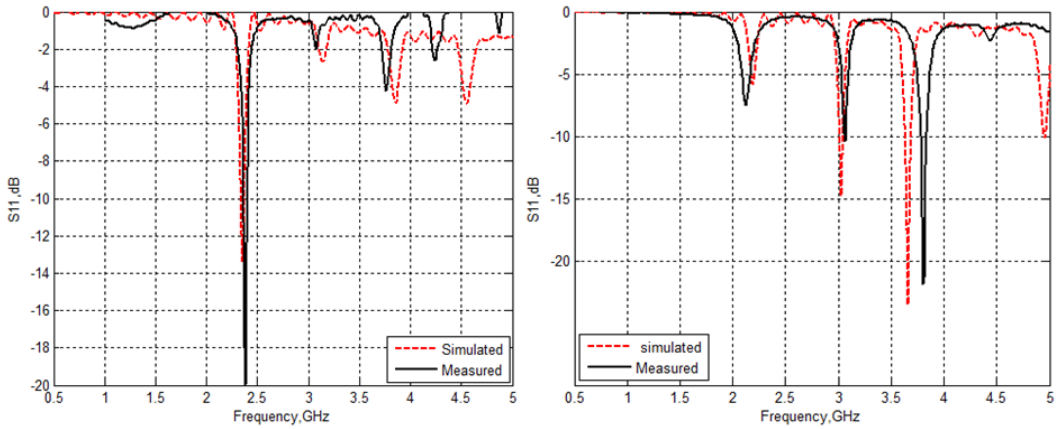


**Figure 7.** Return loss of simulated and measured results of (a) the unit cell CRLH antenna, (b) the one cell CRLH antenna with a small stub.

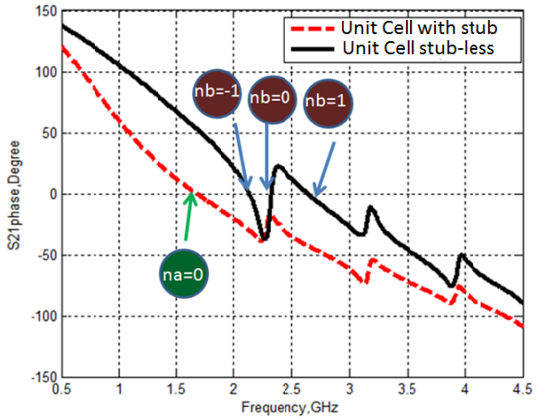


**Figure 8.** The simulated phase of the unit cell transmission coefficient for single stub and stub-less cells.

## 4. QUAD/FIFTH TWO SECTIONS CRLH ANTENNA

Referring to Eq. (11), by increasing the cells number, the possible radiated modes will be introduced in the two antennas. Therefore, in this section, we introduce the comparison between the two cells CRLH with stub and with phase enhanced stub. The two antennas were designed on a substrate FR4 with relative permittivity = 4.4, dielectric loss tangent = 0.025 and thickness ($h$) = 1.6 mm. The feeding for the antenna matches a 50 Ω RH feeding line. Also, the two different CRLH antennas performances were validated by studying the return loss of the antenna employing CST and confirmed using experimental measurement. The two antennas' sizes are equal ($38 \times 22\,\text{mm}^2$).

The first two cells antenna model is based on using two complete left-handed cells antenna with stub lengths shown in Fig. 9(a), and the fabricated antenna is illustrated in Fig. 9(b). The 2D layout of the proposed two left-handed cells antenna is shown in Fig. 10(a), and the fabricated antenna is illustrated in Fig. 10(b).

### 4.1. Two Stub CRLH Cells CRLH Antenna

The simulated reflection coefficient compared to the measured one of the antenna stub CRLH cell is illustrated in Fig. 11. Both results confirm the multi-band resonances compared to only one band in one cell antenna configuration. However, there is a small upper frequency shift (about 0.1 GHz) in

measurement results compared to simulate one. This is mainly due to imperfection in fabrication and connector soldiering process which cannot be totally avoided.

The simulated resonances are at 0.8 GHz with −6 dB reflection coefficient (with $na = -1$ order), at 2.4 GHz with −16 dB reflection coefficient (with $na = 0$), at 3.1 GHz with −13 dB reflection coefficient (with $na = 1$ order), at 3.7 GHz with −13 dB reflection coefficient (with $na = 2$ order) and at 4.4 GHz with −13 dB reflection coefficient (with $na = 3$ order). One resonance is at LH band whose reflection coefficient does not exceed −10 dB. Three resonances are in the right-handed passband with reflection = −13 dB at the three bands.

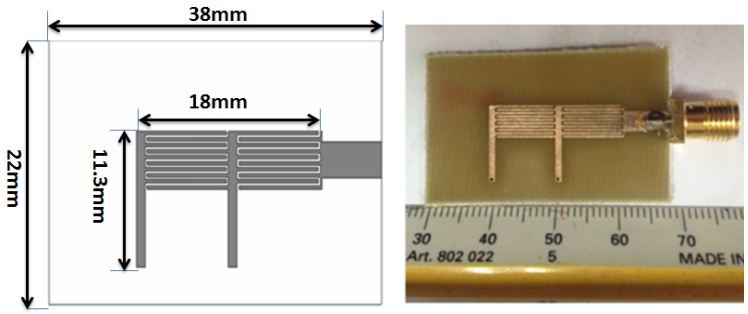


(a) (b)

**Figure 9.** The stub two-cells CRLH antenna. (a) 2D layout. (b) Fabricated antenna.

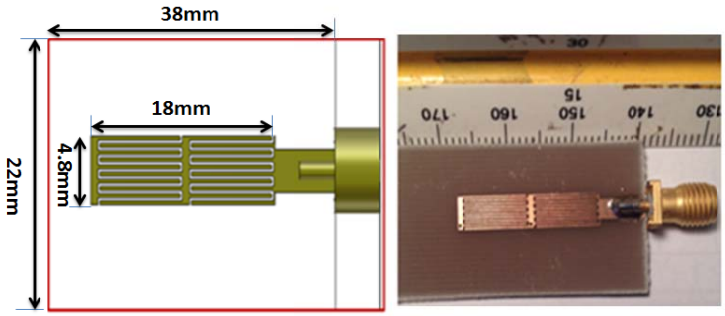


(a) (b)

**Figure 10.** The stub-less two cells CRLH antenna. (a) 2D layout. (b) Fabricated antenna.

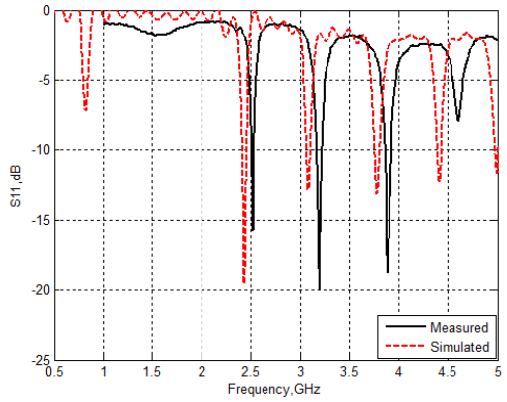


**Figure 11.** Return loss of simulated and measured results of the stub CRLH multi-band antenna.

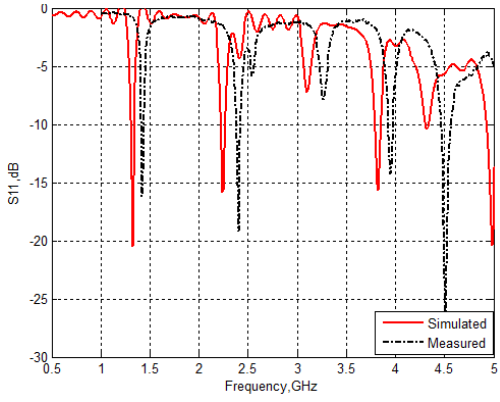


**Figure 12.** Reflection coefficient of simulated and measured results of the stub-less CRLH multi-resonance antenna.

### 4.2. Two Cells with Stub Phase Enhancement CRLH Antenna

The simulated and measured reflection coefficient results of the stub-less CRLH cell antenna are shown in Fig. 12. Both results confirm the multi-resonance (5 resonances). The simulated resonances are at 1.3 GHz, 2.4 GHz, 3.1 GHz, 3.8 GHz and 4.4 GHz with reflection coefficient = −22 dB, −16 dB, −7 dB, −16 dB, and −11 dB, respectively. Similar to the previous measurement, the measured resonance frequencies are shifted up with approximate 100 MHz compared to simulated ones.

Finally, comparison between the proposed antennas and other ZOR metamaterial antennas is illustrated in Table 1.

**Table 1.** Comparison between the proposed antennas and the previous ZOR metamaterial antennas.

| Parameter | Unite cell stub — less | Two cells stub — less | Ref. [23] | Ref. [19] | Ref. [20] |
|---|---|---|---|---|---|
| Operating Frequency | 2.2 GHz, 3 GHz and 3.6 GHz | 1.3 GHz, 2.4 GHz, 3.1 GHz, 3.8 GHz and 4.4 GHz | 1.76 GHz, 2.55 GHz and 3.85 GHz | 1.76 GHz, 1.88 GHz, 2.49 GHz and 2.64 GHz | 3.8 GHz |
| BW (at 10 dB) | 50 MHz and 80 MHz | 33 MHz, 30 MHz, 70 MHz and 10 MHz | 25 MHz, 32 MHz and 100 MHz | 36 MHz, 35 MHz, 37 MHz and 60 MHz | 260 MHz |
| Total Size ($mm^3$) | 28 ×22 × 1.6 | 38 × 22 × 1.6 | 30 × 30 × 1.6 | 40 × 40 × 4 | 40× 35 × 1.6 |
| Polarization | linear | linear | linear | linear | linear |

## 5. CONCLUSION

A nonlinear phase enhancement of multi-resonance CRLH transmission line has been introduced. The non-phase enhanced antenna consists of left-handed cell constructed using series interdigital capacitor and shunt inductor whereas the phase enhanced CRLH antenna consists of series interdigital ended with via. Because of the nonlinearity behavior of the left-handed region of composite right/left-handed transmission line, the proposed antenna has compact size compared to conventional patch antennas operating at the same frequencies. The antenna has been operated at different resonances, which is applied to wireless applications. A good agreement has been achieved between the measured and simulated results.

## REFERENCES

1. Wong, K. L., *Planar Antennas for Wireless Communications*, John Wiley & Sons, Inc., 2003.
2. Song, K., Y.-Z. Yin, and B. Chen, "Triple-band open L-slot antenna with a slit and a strip for WLAN/WiMAX applications," *Progress In Electromagnetics Research Letters*, Vol. 22, 139–146, 2011.
3. Hu, W., Y. Z. Yin, P. Fei, and X. Yang, "Compact triband square-slot antenna with symmetrical L-strips for WLAN/WiMAX applications," *IEEE Antennas and Wireless Propagation Letters*, Vol. 10, 462–465, 2011.
4. Risco, S., J. Anguera, A. Anduar, A. Perez, and C. Puente, "Coupled monopole antenna design for multiband handset devices," *Microwave and Optical Technology Letters*, Vol. 52, 359–364, 2010.
5. Ciais, P., R. Staraj, G. Kossiavas, and C. Luxey, "Design of an internal quad-band antenna for mobile phones," *IEEE Microwave and Wireless Components Letters*, Vol. 14, 148–150, 2004.

6. Caloz, C. and T. Itoh, *Electromagnetic Metamaterials Transmission Line Theory and Microwave Applications*, John Wiley & Sons, New Jersey, 2006.
7. Engheta, N. and R. W. Ziolkowski, *Electromagnetic Metamaterials: Physics and Engineering Explorations*, Wiley, Hoboken, NJ, 2006.
8. Eleftheriades, G. V. and K. G. Balmain, *Negative Refractive Metamaterials*, John Wiley & Sons, New Jersey, 2005.
9. Eleftheriades, G. V., "Enabling RF/microwave devices using negative-refractive-index transmission-line (NRI-TL) metamaterials," *IEEE Antennas and Propagation Magazine*, Vol. 49, No. 2, 34–51, 2007.
10. Caloz, C., "Metamaterial dispersion engineering concepts and applications," *Proceedings of the IEEE*, Vol. 99, No. 10, 1711–1719, 2011.
11. Holloway, C. L., E. F. Kuester, J. A. Gordon, J. O'Hara, J. Booth, and D. R. Smith, "An overview of the theory and applications of metasurfaces: The two-dimensional equivalents of metamaterials," *IEEE Antennas and Propagation Magazine*, Vol. 54, No. 2, 10–35, 2012.
12. Dong, Y. and T. Itoh, "Promising future of metamaterials," *IEEE Microwave Magaz.*, Vol. 13, No. 2, 39–56, 2012.
13. Abdalla, M. A. and Z. Hu, "Compact tunable left handed ferrite transformer," *International Journal of Infrared and Millimeter Waves*, Vol. 30, No. 8, 813–825, 2009.
14. Abdalla, M. A. and Z. Hu, "Compact novel CPW ferrite coupled line circulator with left-handed power divider/combiner," *2011 European Microwave Week, EuMW2011*, 794–707, Digest, Manchester, UK, 2011.
15. Karimian, S., Z. Hu, and M. Abdalla, "Compact half-wavelength metamaterial stepped impedance resonator (SIR)," *IEEE International Symposium on Antennas and Propagation AP-S*, 2951–2953, 2011.
16. Abdalla, M. A., M. A. Fouad, H. A. Elregeily, and A. A. Mitkees, "Wideband negative permittivity metamaterial for size reduction of stopband filter in antenna applications," *Progress In Electromagnetics Research C*, Vol. 25, 55–66, 2012.
17. Abdalla, M. A. and Z. Hu, "On the study of left-handed coplanar waveguide coupler on ferrite substrate," *PIERS Proceedings*, 667–671, Hangzhou, China, Mar. 24–28, 2008.
18. Abdalla, M. A., "Experimental verification of a triple band thin radar absorber metamaterial for oblique incidence applications," *Progress In Electromagnetic Research Letters*, Vol. 39, 63–72, 2013.
19. Segovia-Vargas, D., F. J. Herraiz-Martinez, E. Ugarte-Munoz, L. E. Garcia-Munoz, and V. Gonzalez-Posadas, "Quad-frequency linearly-polarized and dual-frequency circularly-polarized microstrip patch antennas with CRLH loading," *Progress In Electromagnetics Research*, Vol. 133, 91–115, 2013.
20. Ha, J., K. Kwon, Y. Lee, and J. Choi, "Hybrid mode wideband patch antenna loaded with a planar metamaterial unit cell," *IEEE Transactions on Antennas and Propagation*, Vol. 60, No. 2, 1143–1147, 2012.
21. Dong, Y. and T. Itoh, "Metamaterial-based antennas," *IEEE Proceedings*, Vol. 100, No. 7, 2271–2285, 2012.
22. Mehdipour, A. and G. V. Eleftheriades, "Leaky-wave antennas using negative-refractive-index transmission-line metamaterial supercells," *IEEE Transactions on Antennas and Propagation*, Vol. 62, No. 8, 3929–3942, 2014.
23. Rahimi, M., F. B. Zarrabi, R. Ahmadian, Z. Mansouri, and A. Keshtkar, "Miniaturization of antenna for wireless application with difference metamaterial structures," *Progress In Electromagnetics Research*, Vol. 145, 19–29, 2014.
24. Abdalla, M. A. and Z. Hu, "A compact dual band meta-material antenna for wireless applications," *2012 Loughborough Antennas & Propagation Conference*, 1–4, UK, 2012.
25. Abdalla, M., S. Karimian, and Z. Hu, "Dual band spurious-free SIR metamaterial antenna," *IEEE AP-S International Antenna and Propagation Symposium Digest*, 1005–1006, Memphis, USA, 2014.

26. Abdalla, M., "A dual mode CRLH TL metamaterial antenna," *2014 IEEE AP-S International Antenna and Propagation Symposium Digest*, 793–794, Memphis, USA, 2014.
27. Abdalla, M. A., U. Abdelnaby, and A. A. Mitkees, "Compact and triple band meta-material antenna for all WiMAX applications," *ISAP Int. Symp. Dig.*, 1176–1179, 2012.
28. Abdalla, M., M. Abo El-Dahab, and M. Ghouz, "Dual/triple band printed dipole antenna loaded with CRLH cells," *IEEE AP-S Int. Symp. Dig.*, 1007–1008, Jul. 2014.
29. Pozar, D. M., *Microwave Engineering*, 4th Edition, J. Wiley & Sons, New York, 2012.
30. Shen, J., G. Hong, and M. J. Lancaster, *Microstrip Filters for RF/Microwave Applications*, 2nd edition, Wiley, 2004.